Applied Catalysis B: Environmental 321 (2023) 122049

Contents lists available at ScienceDirect

Applied Catalysis B: Environmental

journal homepage: www.elsevier.com/locate/apcatb

Tuning band structures of Hf-PCN-224(M) for β-Carbonyl C(sp^3)-H bond activation and difunctionalization: Tandem C(sp^3) radical cross-coupling through photoredox

Lingjuan Zhang [a], Lijuan Ma [a], Jincong Yuan [a], Xian-Ming Zhang [a,b,*], Zhiyong Tang [c,d]

[a] Key Laboratory of Magnetic Molecules and Magnetic Information Materials (Ministry of Education), School of Chemistry and Material Science Shanxi Normal University, Taiyuan, Shanxi 030006, PRChina
[b] College of Chemistry, Key Laboratory of Interface Scienceand Engineering in Advanced Material (MOE) Taiyuan University of Technology, Taiyuan, Shanxi 030024, PR China
[c] CAS Key Laboratory of Nanosystem and Hierarchical Fabrication, CAS Center for Excellence in Nanoscience, National Center for Nanoscience and Technology Beijing, 100190, PR China
[d] University of Chinese Academy of Sciences, Beijing 100049, PR China

ARTICLE INFO

Keywords:
Band structure
Photoredox
C(sp^3)-H bond activation
Radical-radical cross-coupling
Difunctionalization

ABSTRACT

The construction of C(sp^3)-C(sp^3) bonds by different C(sp^3) radicals coupling reactions is still unexplored due to the high bond dissociation energy of C(sp^3)-H bond and the difficulty for selective generating of C(sp^3) radical. Benefiting from the precisely regulating for band structures of Hf-PCN-224(M), the β-carbonyl C(sp^3)-H bonds are effectively oxidized by photo-generated holes to affording C(sp^3) radicals in this work. C(sp^3)-C(sp^3) and C(sp^3)-O bonds are constructed by tandem radical-radical cross-coupling, hydrogen atom transfer (HAT), and radical-radical cross-coupling between two C(sp^3)-H bonds, enabling an effective C_3-difunctionalization of indolin-2-ones under photo-thermo synergetic catalysis on Hf-PCN-224(Cu). Significantly, OH serves as triple roles: introduced hydroxyl group in situ, HAT abstractor and α-heteroatom for secondary activating C(sp^3)-H bonds. Control experiments, EPR spectroscopy and DFT calculation provide insight into the tandem radicals cross-coupling mechanism. This operable strategy opens up a door for the difunctionalization of C(sp^3)-H bonds in heterogeneous photoredox manner.

1. Introduction

The coupling of C(sp^3) radicals to constructing C(sp^3)-C(sp^3) bonds is a long-standing scientific issue, especially by cross-coupling of different C(sp^3) radicals [1]. How to manufacture targeted radicals effectively and selectively is the main challenge. Clearly, C(sp^3)-H bonds are the most ideal source of C(sp^3) radicals from the atomic economics standpoint, [2] however, the core issue in this field is how to overcome high bond dissociation energy of C(sp^3)-H bond [3]. Traditionally, the cleavage of aliphatic C-H bonds for delivering C(sp^3) radicals is feasible in thermochemical manner. However, it is inevitable to use toxic organotin reagents, high temperatures, or excess peroxides or persulfates, resulting in the energy-intensive and uncontrollable side reactions.[4] Photocatalytic C(sp^3) radical production is more appealing and promising in the realm of organic transformations due to its tunable on-target radical species, limited off-target radical couplings and mild conditions. [1,5,6] Using rare Ir/Ru complexes as homogeneous photo-catalysts to promote electrophilic O/N/S/X/C-centered radicals as hydrogen atom transfer (HAT) abstractors can release C(sp^3) radicals, in which excess additives (e.g. peroxides/persulfates/phosphates/RSH, etc.) are necessary in general (Scheme 1a) [7,8].

In contrast, the activation and cleavage of C(sp^3)-H bonds through photo-generated hole (h^+) oxidation of heterogeneous photocatalyst provides a powerful alternative to afford C(sp^3) radicals [9]. In 2021, Wu's group revealed that the coupling reactions of C(sp^3) radicals generated from α-oxy/allylic C(sp^3)-H bonds by h^+ oxidation of CdSe quantum dots, which effectively constructed the C(sp^3)-C(sp^2), C(sp^3)-S and C(sp^3)-C(sp^3) bonds. H_2 as by-product was generated by the photo-generated electron (e^-) reduction to the proton released from C (sp^3)-H bond in argon atmosphere [10]. It is well known that the

* Corresponding author at: Key Laboratory of Magnetic Molecules and Magnetic Information Materials (Ministry of Education), School of Chemistry and Material Science Shanxi Normal University, Taiyuan, Shanxi 030006, PRChina.
E-mail addresses: zhangxm@dns.sxnu.edu.cn (X.-M. Zhang), zytang@nanoctr.cn (Z. Tang).

https://doi.org/10.1016/j.apcatb.2022.122049
Received 25 August 2022; Received in revised form 2 October 2022; Accepted 3 October 2022
Available online 4 October 2022
0926-3373/© 2022 Elsevier B.V. All rights reserved.

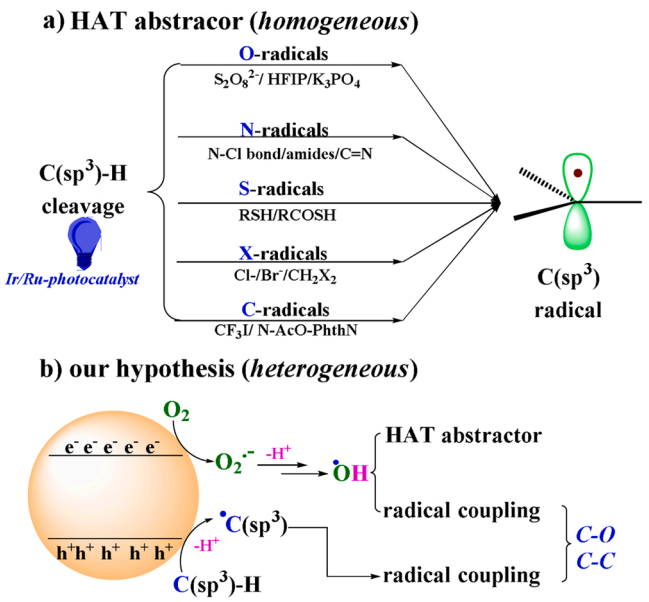

Scheme 1. The cleavage of C(sp^3)-H bonds for generating C(sp^3) radicals through photocatalysis.

versatile reactive oxygen species (ROS, e.g. •OH, H_2O_2, $^1O_2$, $O_2^{\bullet-}$, etc.) can be obtained from O_2 reduced by photo-generated e^- [11]. However, using ROS (e.g. •OH) as HAT abstractor is still lacking in the research of C(sp^3) radicals fostering. Moreover, the multi-functionalization of C (sp^3)-H bond remains undeveloped via tandem radical-radical cross--coupling manner over heterogeneous photoredox.

Metal-organic frameworks (MOFs) with tunable light absorption and homogeneous/explicit catalytic sites for analyzing structure-property relationships, have been widely explored as photocatalysts in the organic transformations [12]. Yang and Schröder group reported the photo-reductive coupling of aldehydes or ketones over hydroxyl-decorated MFM-300(Cr) with Na_2SO_3 as reducing agent [13]. Recently, our group reported efficient asymmetric alkylation of aldehyde C-H groups with benzyl halides via photo-catalytic radical cross-coupling over chiral MOFs, in which the benzyl radicals were obtained by the reduction of light-induced electrons to C—Br bonds [14]. The chem- and stereo-selective coupling reactions could be achieved by tuning the chiral catalytic sites, but triethanolamine was necessary as electron sacrificial agents. Obviously, the multiple-sites synergistic catalyzed performance and precise control for product selectivity can be well tuned by changing the electronic structures, geometric structures and surface chemical micro-environment of MOFs, which are similar to the characteristic of enzymes.[15] In this context, it is feasible to develop MOFs-based photo-catalytic platforms for C(sp^3)-H multi-functionalization based C(sp^3) radicals cross-coupling in the presence of O_2. It is expected that ROS can serve as a potent HAT abstractor and oxygen source for oxy-functionalization when h^+ oxidation is used to cleave C(sp^3)-H bonds (Scheme 1).

C_3-difunctional indolin derivatives are prominent moieties in many antimicrobial, antitumor and anti-HIV drugs, such as donaxaridine, convolutamydine A and Maremycin B [16] Transition metal-catalyzed C (sp^3)-H difunctionalization of indolin-2-one has been achieved involving radicals; [17] however, it still remains elusive through tandem C(sp^3) radicals cross-coupling via heterogeneous photoredox pathway. In this work, the effective activation and difunctionalization of β-carbonyl C (sp^3)-H bonds has been realized with high yields and good selectivities with semiconductor-like porphyrin-based PMOF, Hf-PCN-224(Cu), as heterogeneous photocatalyst. This work shows the following highlights: (1) selective C(sp^3) radicals generation through h^+ oxidation based on precise tuning of band structure; (2) tandem $^{\bullet}C_{indolin}$-$^{\bullet}OH$ cross-coupling/HAT/$^{\bullet}C_{indolin\text{-}O}$-$^{\bullet}C_{quinoline}$ cross-coupling for the C_3-difunctionalization of indolin-2-ones; (3) triple roles of OH: introduced hydroxyl group in situ for radical coupling, α-heteroatom for secondary activating C(sp^3)-H bonds and HAT abstractor; (4) fast transfer of photo-generated electron to Cu(II) site of porphyrin ring, which suppresses e^--h^+ recombination; (5) photo-thermo synergistic working of PMOF; (6) no use of sacrificial electron donors; (7) high turnover frequency (TOF) value up to 28 times that of the corresponding homogeneous CuTPPM (CuTPPM = Cu-Tetrakis (4-methoxycarbonylphenyl) porphyrin) system.

2. Experimental procedures

2.1. Synthesis of Hf-PCN-224(Cu, 1200 nm) [18]

Hf-PCN-224 (Cu, 1200 nm) was synthesized according to a reported procedure with slight modification. $HfCl_4$ (50 mg) was dissolved in 7 mL of DMF under ultrasonication for 30 min. The solution was transferred to a 20 mL Teflon-lined steel autoclave, and tightly sealed before heating 80 °C for 1 h in oven. After cooling to room temperature, the solution of CuTCPP (25 mg) dissolved in 3 mL DMF was dropwise added into the above mixture and sonicated for 10 min. Then, the mixture was tightly sealed and heated 120 °C. After 2.5 h, red crystals were obtained, washed with DMF and methanol several times and dried.

2.2. Characterizations

Single crystal of Hf-PCN-224(Cu) with appropriate dimensions was chosen under an optical microscope and quickly coated with high vacuum grease (Dow Corning Corporation) to prevent decomposition. Crystal was mounted on CryoLoop loop and the cell parameter and intensity data were recorded on a Rigaku Oxford Diffraction XtaLAB Synergy-S diffractometer equipped with a HyPix-6000HE Hybrid Photon Counting (HPC) detector operating in shutterless mode and an Oxford Cryosystems Cryostream 800 Plus at 150 K using Cu Kα (λ = 1.54184 Å) for Hf-PCN-224(Cu) from PhotonJet micro-focus X-ray Source. Data were processed using the CrystAlisPro software suite. Absorption corrections were applied by using the program CrysAlisPro (multi-scan). Crystal structure was examined using the Addsym subroutine of PLATON to ensure that no additional symmetry could be applied to the models. The structure was solved with direct methods and refined using Full-matrix least-squares based on F2 with program SHELXL-97 within OLEX 2. PXRD patterns were measured on Rigaku D/Max-2500 diffractometer with Cu target tube at 40 kV and 30 mA. The UV–vis spectra of the samples were measured on a UV–vis spectrophotometer (LAMBDA650) and $BaSO_4$ was used as the reflectance standard reference. The morphology analysis of the as-prepared samples was conducted on a scanning electron microscope (SEM, S4800, Hitachi Co., Japan). TEM, HAADF-STEM, and elemetal mapping images were taken on a transmission electron microscope (TEM, 2100 F, JEOL Co., Japan). Nitrogen adsorption–desorption isotherms and BET surface areas were recorded using a Micrometritics ASAP 2420 system at 77 K, and the pore size distributions were analyzed by density functional theory (DFT) model. Before nitrogen adsorption–desorption measurement, the samples were treated under vacuum at 120 °C for 12 h. The PL spectra of samples and the PL lifetime were recorded on the powder samples by using Edinburgh FLS920 fluorescence spectrometer with a picosecond pulsed diode laser. X-ray photoelectron spectroscopy (XPS) was carried out on a Thermo Fisher SCIENTIFIC using Al Kα X-ray source. Binding energies (BE) were calibrated by setting the measured BE of C_{1s} to 284.65 eV. Thermogravimetric analyses (TGA) were performed on Shanghai yinnuo 1000 B under O_2 atmosphere at a heating rate of 10 °C min^{-1}.

2.3. Electrochemical measurements

Photocatalyst (2 mg) was well dispersed in 1 mL ethanol containing 10 μL nafion and sonicated for 30 min. Next, 200 μL above suspension was dispersed dropwise onto the surface of a clear ITO glass with exposed 1 × 1 cm^2 area. After drying overnight in oven, the loading mass was about 0.4 mg/cm^2.

The photoelectrochemical measurements were carried out in CHI-660 electrochemical station (Chenhua instrument, Shanghai, China). The as-synthesized photoanode of Hf-PCN-224(Cu)/Hf-PCN-224 was used as working electrode in a common three electrode configuration with Pt foil as the counter electrode and Ag/AgCl (saturated KCl) as the reference electrode. Na_2SO_4 (0.2 M) solution was used as the electrolyte and Xe lamp (300 W, $\lambda \geq 380$ nm, CEL-HXE 300, Beijing China Education Au-light Technology Co., Ltd.) was used as the light source. The photocurrent response was measured at + 0.4 V bias voltage under chopped light and the Mott-Schottky plots were tested in the dark at 300/500/1000 Hz. The electrochemical impedance spectroscopy (EIS) measurement was performed in the frequency range from 10^{-2} to 10^5 Hz with a bias potential of 1.75 V.

2.4. Computational details

The DFT calculations were performed with the Becke's three-parameter hybrid method with the Lee, Yang and Parr (B3LYP) gradient-corrected correlation functional [19,20]. The all-electron basis set 6–31 +G*[21] was adopted for all atoms. Spin multiplicities, zero point energies (ZPEs) and Gibbs free energy corrections were obtained at the same level. The structures were optimized without any symmetry constraints. We also performed normal-mode frequencies calculations to ensure that the stable geometries were energy minima without imaginary frequencies.

2.5. Photocatalytic experiments

In a typical experiment, Hf-PCN-224 (Cu, 5 mg) was added in a mixture of DMF (1 mL), indolin-2-one (**1a**, 0.2 mmol) and 2-methylquinoline (**2a**, 0.22 mmol). Under O_2 atmosphere, the reaction was heated to 80 °C in a 5 mL branched Schlenk tube with gentle stirring, irradiated with a 300 W Xe lamp equipped with a UV cut-off filter ($\lambda \geq 380$ nm) and monitored by TLC. After indolin-2-one (**1a**) was exhausted completely, the reaction was cooled down to room temperature and quenched in saturated NaCl solution (10 mL), then extracted with EtOAc (3 × 10 mL). The catalyst was separated by centrifugation, thoroughly washed with ethanol, and then reused in subsequent runs. The combined organic layers was concentrated in vacuo, then the residue was purified by flash column chromatography (petroleum ether: ethyl acetate = 2: 1) to get oxidative-coupling product **3a** as off-white powder.

3. Results and discussion

3.1. Synthesis and characterizations of Hf-PCN-224 (Cu)

Solvothermal treatment is used to yield dark red colored crystals of Hf-PCN-224 (Cu) with different sizes in DMF solution on the basis of precursors including $HfCl_4$, CuTCPP and acid regulator. The structure of Hf-PCN-224 (Cu) is confirmed by single-crystal X-ray diffraction and powder X-ray diffraction tests, which is in good agreement with the reported Zr/Hf-PCN-224 (Figs. S1 and S2).[22] Noted that the crystallinity lowers along with the decrease of sample sizes (Fig S2). Scanning electron microscopy (SEM) measurement shows a series of changes of Hf-PCN-224 (Cu) about the morphology, which are from cube to spheres to irregular particles along with the size decreasing from 3 μm to 200 nm (Fig. S3). The high-angle annular dark-field scanning TEM (HAADF--STEM) image and the corresponding elemental mapping analysis of Hf-PCN-224 (Cu, 1200 nm) indicate uniform distributions of elements C, O, N, Cu and Hf throughout the sphere (Fig. 1).

To further analyze Hf-PCN-224 (Cu, 1200 nm), some related measurements are utilized here. The N_2 adsorption of Hf-PCN-224 (Cu, 1200 nm) exhibits a typical type I isotherms with N_2 uptake of 565 cm^3/g at 1 bar, with Brunauer-Emmett-Teller (BET) surface area of 1723 m^2/g and pore size of 2.0 nm (Fig. S4). Thermogravimetric analysis under air atmosphere shows an excellent thermal stability up to 400 °C, which is beneficial for the thermal catalytic application of Hf-PCN-224(Cu) (Fig. S5). Furthermore, the X-ray photoelectron spectroscopy (XPS) spectrum of the Hf-PCN-224 (Cu) clearly shows signals of Cu^{2+} at 934.9 and 954.8 eV (Fig. 2a). A prominent band located at 398.5 eV is observed in the N 1 s region, indicating that all nitrogen atoms are coordinated with Cu^{2+} in porphyrin ring (Fig. S6). The Cu loading in Hf-PCN-224(Cu) is shown to be 3.3 wt% as measured by inductively coupled plasma mass spectrometry (ICP-MS).

3.2. Photo-physical Investigation of Hf-PCN-224 (Cu)

The strong absorption in the solid-state UV-Vis spectra indicates an excellent photon absorption in the visible light range (Fig. S7a). The Tauc plot discloses an optical band gap of 1.9 eV (Fig. S7b). According to the Mott-Schottky (MS) curves collected at frequencies of 300, 500, and 1000 Hz, the flat potential is identified as − 0.7 V vs. Ag/AgCl (Fig. S8) and the positive slope of the MS plot is observed, which elucidates the *n*-type semiconductor character of Hf-PCN-224 (Cu). Thus, the conduction band (LUMO) and valence band (HOMO) level are calculated as.

-0.74 and 1.16 V (vs. SCE), respectively (Fig. 2b). It is clearly noticed that the transient photocurrent response of Hf-PCN-224 (Cu) is enhanced compared to that of Hf-PCN-224 under visible light irradiation, implying that the generation of electron-hole (e^--h^+) pairs and photoelectrical performance are improved after implanting Cu(II) in the center of porphyrin ring (Fig. 2c). Moreover, the decreased impedance of Hf-PCN-224 (Cu) favors the transfer of photo-generated electrons (Fig. 2d).[23] Overall, the excellent photo-physical behaviors of Hf-PCN-224 (Cu) show great potential as a photocatalyst.

3.3. Photo-catalytic oxidative-cross coupling

To date, the synthetic methods of C_3-difunctionalized indolin derivatives mainly rely on (i) the C_3-site addition of isatins, including aldol reaction and henry reaction;[24] (ii) the hydroxylation/alkylation of 3-substituted-2-oxindoles;[25] (iii) the cross-coupling reaction of C(sp^3)-H bonds.[17] The last method is more appealing since it avoids pre-functionalized substrates and accomplishes oxidative-coupling in one-pot. Herein, the excellent photoelectrical properties of Hf-PCN-224 (Cu) promote us to explore the photo-catalytic performance for the activation and cleavage of β-carbonyl C(sp^3)-H bonds to afford C(sp^3) radicals.

As a proof of concept, the cross-coupling of indolin-2-one 1a and 2-methylquinoline 2a is employed as a model reaction and a series of probe tests (Table 1). (1) A metallic ion at the porphyrin center is required, and the coupling product 3a exhibits the best chem-selectivity with Hf-PCN-224 (Cu) as catalyst (entries 1–4). (2) The oxidative coupling is inert in the absence of O_2 and mild heating (entries 5–7). (3) Nano-grade Hf-PCN-224(Cu) shows more efficient catalytic performance than block crystals, which benefits from efficient mass transfer. It is found that the highest TOF value and yield are obtained when PCN-224 (Cu, 400–800 nm) is used (entry 11). However, the continuous reducing of catalyst size (200–300 nm) results in the decreasing of the yield of 3a due to the particle conglobation effect during reaction process (entry 12). (4) Both the reactant concentration and the contact chance of active intermediates are enhanced by the hydrogen bonding between the reactants and terminal -OH groups on the Hf nodes [26]. Therefore, the high chem-selectivity of 3a and TOF value of catalyst can be achieved, especially using nano-grade PCN-224 (Cu) as catalyst, which is up to 28–31 times that of the corresponding homogeneous

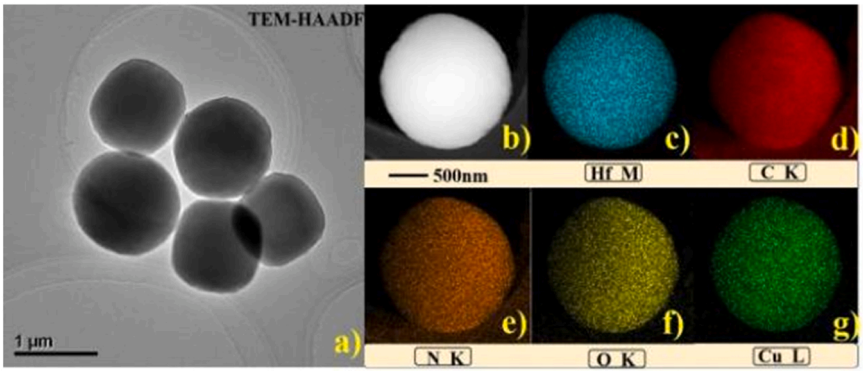

Fig. 1. HAADF-STEM image and corresponding elemental mapping images of Hf-PCN-224 (Cu).

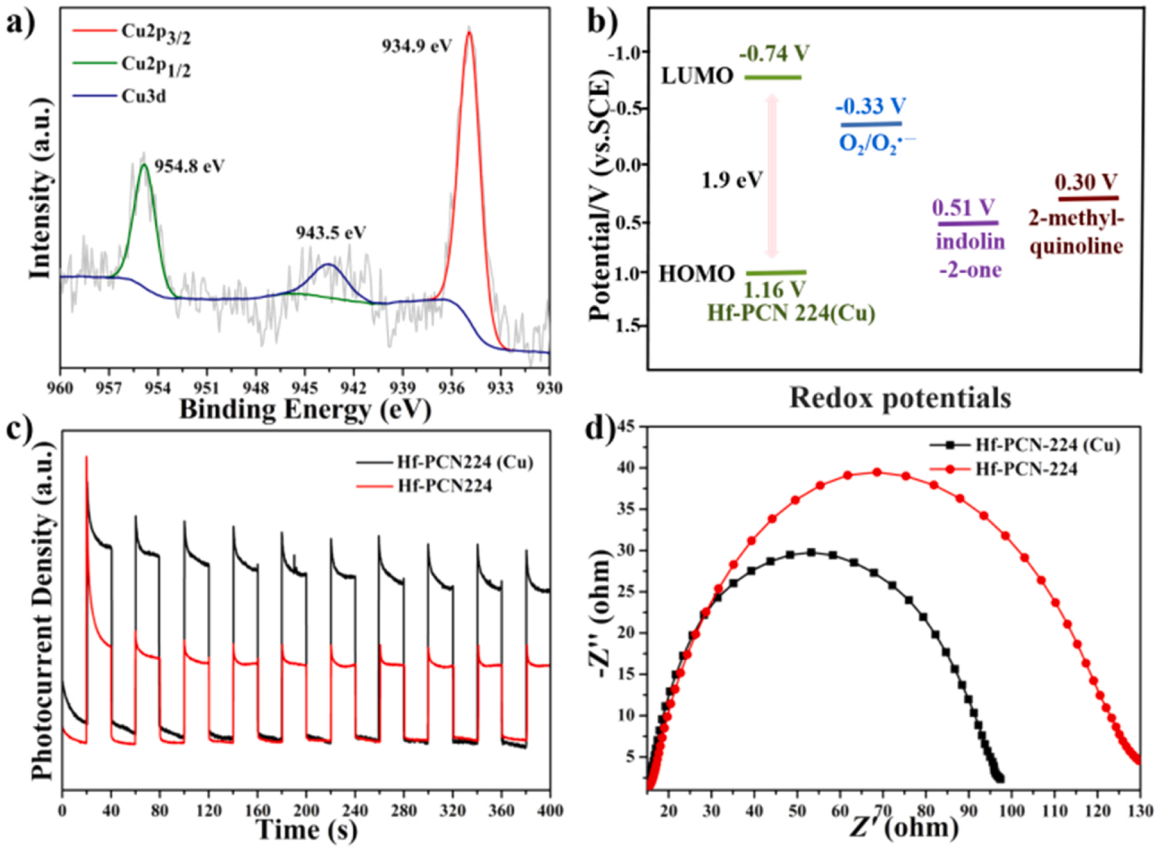

Fig. 2. a) High resolution Cu XPS spectrum of Hf-PCN-224(Cu) Sample; b) the HOMO-LUMO positions of Hf-PCN-224(Cu), and the redox potentials of 1a and 2a; c) Transient photocurrent response; d) Electrochemical impedance spectra of Hf-PCN-224(Cu) and Hf-PCN-224, respectively.

catalyst CuTPPM and 14–15 times of $Fe(OAc)_2$ (entries 13–14) [17].

3.4. mechanism of the photocatalytic cross coupling reaction

To shed light on the catalytic mechanism, several related tests for catalysts are carried out. (1) Based on the MS plots and cyclicvoltammetry (CV) analysis, the HOMO value (1.16 V, vs. SCE) of Hf-PCN-224 (Cu) is more positive than the redox potential of 1a and 2a (0.51 V, 0.30 V vs. SCE, respectively), and the LUMO value (−0.74 V, vs. SCE) is more negative than the redox potential of $O_2/O_2^{\bullet-}$(−0.33 V, vs. SCE), implying that the sample is suitable for the aerobic photo-oxidative coupling (Fig. 2b and S8). By comparison, the HOMO value (0.42 V, vs. SCE) of Hf-PCN-224(Ni) is too low to oxidize 1a (Figs. S9a, 9b and S10). Regarding to Hf-PCN-224(Fe), the values of HOMO and LUMO are close to the redox potential of 1a and 2a, which displays poor redox activity in the cross-coupling reaction (Figs. S9c, 9d and S10). (2) After Cu(II) modification, the obvious PL emission quenching phenomena and slightly shortened fluorescence lifetime indicate that photo-generated electrons from the conduction band of Hf-PCN-224 can be captured by Cu(II) site, which suppresses effectively recombination of e^--h^+ pairs (Fig. S11). (3) The radical pathway is proved through adding 2,2,6,6-Tetramethylpiperidine (TEMP) or 1,1-diphenylethylene (DPE) as the radical scavenger (Fig. 3a). Furthermore, by adding KI as hole scavenger, benzoquinone (BQ) as superoxide scavenger, and coumarin (Cou.) as $^{\bullet}OH$ scavenger, lower yields of 42%, 32% and 35% are observed, respectively, indicating that h^+, $O_2^{\bullet-}$ and $^{\bullet}OH$ play critical roles in the photo-catalytic cycle. Moreover, electron paramagnetic resonance (EPR) trapping experiment is performed using 5,5-dimethyl-1-pyrroline

Table 1
Optimization of the reaction condition.[a].

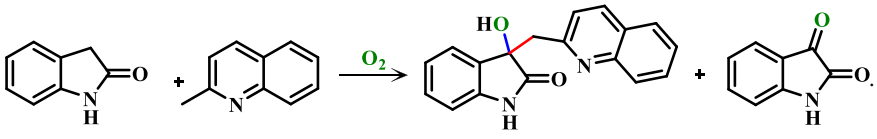

Entry	Catalyst		Size (nm)	Time (h)	Results (%)[b]		TOF (h^{-1})	Comparison of TOF
					3a	4a		
1	PCN-224(Cu)	3 mg	block	48.0	95	trace	–	–
2	PCN-224(Fe)	3 mg	block	48.0	66	30	–	–
3	PCN-224(Ni)	3 mg	block	48.0	50	46	–	–
4	PCN-224	3 mg	block	48.0	trace	3	–	–
5[c]	PCN-224(Cu)	3 mg	block	48.0	trace	trace	–	–
6[d]	PCN-224(Cu)	3 mg	block	48.0	20	3	–	–
7[e]	PCN-224(Cu)	3 mg	block	48.0	trace	3	–	–
8	PCN-224(Cu)	6 mg	block	20	95	trace	–	–
9[f]	PCN-224(Cu)	6 mg	block	11.5	94	trace	8.30	12.02
10[f]	***PCN-224(Cu)***	***6 mg***	***1200***	***5.0***	***96***	***trace***	***19.50***	***28.26***
11[f]	***PCN-224(Cu)***	***6 mg***	***400–800***	***4.5***	***96***	***trace***	***21.65***	***31.39***
12[f]	PCN-224(Cu)	6 mg	200–300	8.0	85	13	10.77	15.61
13[f]	CuTPPM		–	48.0	61	33	0.69	1
14	$Fe(OAc)_2$	10 mol%	–	5.0	93	trace	1.86	2.7

Reaction condition: **1a** (0.2 mmol), **2a** (0.24 mmol, 1.2 eq), DMF (1 mL), 80 °C, white LED light, O_2 ball; *[b]* Isolated yields; *[c]* N_2 atmosphere; *[d]* In dark; *[e]* 50 °C; *[f]* 300 W Xe lamp with a UV-cut off filter, λ > 380 nm;

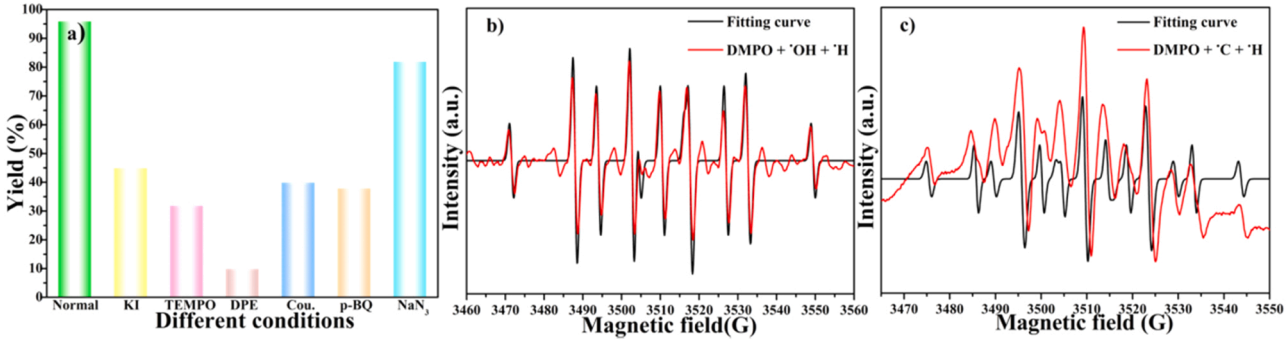

Fig. 3. a) Control experiments; b) DMPO-$^{\bullet}$OH and DMPO-$^{\bullet}$H spin-trapping EPR spectra; c) DMPO-$^{\bullet}C_{indolin\text{-}O}$ and DMPO-$^{\bullet}$H spin-trapping EPR spectra;.

N-oxide (DMPO) as $^{\bullet}$OH trapping agent. The DMPO-$^{\bullet}$OH adduct can be clearly determined in Fig. 3b. (4) Importantly, the signal DMPO-$^{\bullet}C_{indolin\text{-}O}$ adduct (g = 2.006, a_N = 14.4 G, a_H = 19.0 G) is also detected (Fig. 3c). (5) Remarkably, HAT is experienced in the coupling process because DMPO-$^{\bullet}$H (g = 2.006, a_N = 14.2 G, a_H= 20.0 G) adduct is also found (Figs. 3b and 3c). (6) Although the signal of TEMP-$^1O_2$ adduct is obviously determined, $^1O_2$ isn't the key active oxygen species because a slightly reduced yield of 3a is obtained after adding NaN_3 as single oxygen scavenger (Fig. 3a and Fig. S12). (7) Replacing 1a with isatin, only 30% yield of 3a is obtained under the optimal reaction condition for

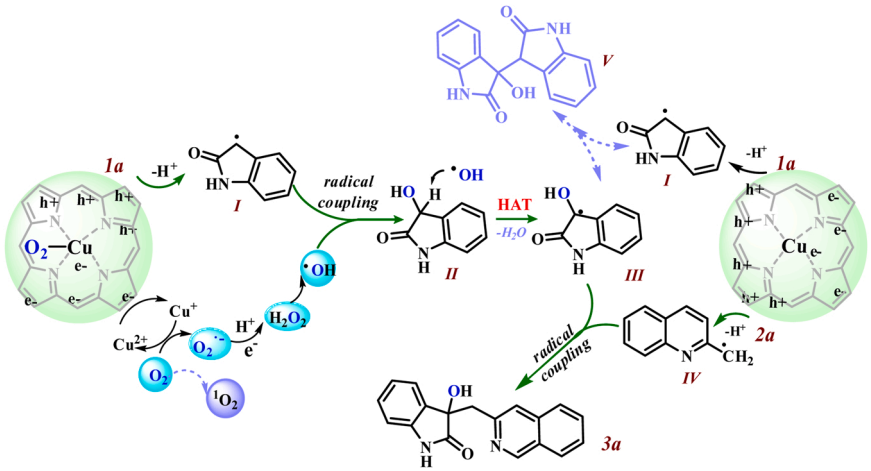

Scheme 2. Possible mechanism.

48 h. The result suggests that isatin, which can be obtained through the oxidation of 1a, is not the key intermediate in the catalytic reaction (Fig. S13).

According to experimental characterization, control experiments, and DFT calculation analysis, a viable mechanism for the photo-thermo synergistic transformation over Hf-PCN-224(Cu) is proposed in Scheme 2. Initially,

Hf-PCN-224(Cu) is photo-excited and the electron-hole pairs are generated upon irradiation. Subsequently, the photo-generated electrons are rapidly transferred from the porphyrin ring to the Cu(II) centers; and simultaneously, Cu(II) is reduced to Cu(I). Next, the dioxygen molecule is reduced to superoxide $O_2^{\bullet-}$ and the Cu(II) is regenerated at the same time. During this process, the direct hole oxidation of indolin-2-one **1a**, which is adsorbed with the Gibbs energy − 19.65 eV (Scheme 3) and activated by copper-porphyrin unit, can provide the radical species $^{\bullet}C_{indolin}$ **I** along with the release of H^+ (ΔG, −17.39 eV). The combination of superoxide $O_2^{\bullet-}$, H^+ and e^- can form H_2O_2, and then O-O homolytic cleavage of H_2O_2 affords radical $^{\bullet}OH$ groups (Fig. 3b). Next, the cross-coupling of $^{\bullet}OH$ and radical **I** generates immediately (ΔG, −30.94 eV). The hydrogen atom transfer of **II** abstracted by $^{\bullet}OH$ affords the carbon radical $^{\bullet}C_{indolin\text{-}O}$ **III** (ΔG, −15.89 eV), accompanied by a H_2O release. Subsequently, the quinoline 2-methylene radical **IV** afforded through the oxidation of **2a** by photo-generated h^+, is coupled with carbon radical **III** to obtain the C_3-difunctionalized indolin-2-one 3a. The calculated barrier of 4.11 eV (3a) exhibits that the cross-coupling reaction is an endothermic process, in well agreement with our photo-thermo synergistic experimental results. In addition, the production of oxidative homo-coupling intermediate **V**, which is successfully and quantitatively converted into products 3a, indicates the formation of radicals **I** and **III** (Fig. S13c). Refer to literature report,[17] we speculate another possible pathway, in which the carbon radical **III** attacks 2a' and affords radical **IV**' (Fig. S14). Afterwards,

$^{\bullet}OH$ acts as the HAT reagent and abstracts $^{\bullet}H$ from **IV**' to form the target product 3a. However, the optimal structure of radical **IV**' could not be found during the process of DFT calculation analysis (Fig. S15). Thus, this reaction pathway is not supported in this work on the basis of the above discussion.

3.5. Scope of the radical-radical cross coupling reaction

It is worth noting that the photo-thermo synergistic cross-coupling reaction by Hf-PCN-224(Cu) is widespread. The indolin-2-ones with electron-withdrawing or electron-donating substituents at different positions of phenyl rings show good compatibility and afford the desired products in high yields (Table 2, 3a-3 h). In addition, the electronic effect of substituent on aromatic ring of 2-methylquinoline does not significantly affect the yields and product selectivity (3i-3 m). However, 4-Cl-2-methylquinoline is less reactive, only giving the coupling product in moderate.

yield (**3 n**, 42%). Strikingly, 2-methylquinoxalines are competent well in the coupling transformations with good yields (**3o-3q**), and the products **3o-3q** are the key precursors of anti-neuroblastoma agent. It is noticed that bathocuproine (2,9-dimethyl-4,7-diphenyl-1,10-phenanthroline) is inert to transformation (**3o**), which also indicates that the heterogeneous oxidative-coupling occurs in the pore of PCN-224 (Cu). After eight runs, the conversion of **1a** and the yield of **3a** are well maintained under the optimized condition (Fig. S16). Furthermore, the invariable PXRD peak, SEM pattern of used Hf-PCN-224 (Cu, Fig. S17) and the low amount of Cu leaching (< 0.01%) into the reaction mixture indicate that the special stability of the photo catalyst is absolutely reliable.

3.6. The derivatization of the C_3-difunctionalized indolin-2-ones products

The 3′-(quinoxalin-2-yl)spiro[indoline-3,2′-oxiran]− 2-one derivatives possess a wide spectrum of anti-neuroblastoma activity.[27] The conventional method is the addition of expensive 2-(dibromomethyl)quinoxaline to isatin derivatives at minus 20 °C, by which oxiranes can be obtained in medium yields. As shown in Scheme 4, spiro [indoline-3,2′-oxiran]− 2-one frameworks are conveniently prepared from C_3- difunctionalized indolin-2-ones **3** in two steps. Treatment of **3o-3q** with *p*-toluene sulfonic acid afford dehydration products **6o-6q** in good yields; 3′-(quinoxalin-2-yl)-spiro[indoline-3,2′-oxiran]− 2-one derivatives **7o-7q** are then obtained with excellent yields through the epoxidation with H_2O_2, respectively.

4. Conclusions

In conclusion, an ultra-efficient strategy for β-carbonyl C(sp^3)-H activation and selective C(sp^3) radical generation is achieved by using Hf-PCN-224(Cu) as photocatalyst. Based on the well-tuned band structure and particle size of Hf-PCN-224(Cu), the C(sp^3)-H difunctionalizations of indolin-2-ones are accomplished through the sequential $^{\bullet}C_{indolin}$-$^{\bullet}OH$ cross-coupling/HAT/$^{\bullet}C_{indolin\text{-}O}$-$^{\bullet}C_{quinoline}$ cross-coupling toward excellent yields and high TOF values. Mechanistic studies disclose that the C(sp^3) radicals are derived from the h^+ oxidation and HAT with in situ introduced $^{\bullet}OH$ as abstractor under photo-thermo synergistic conditions. The protocol features simple operation, readily feedstocks, green oxidant, unused electron sacrificial agents and value-added products. We believe that this strategy not only develops a new mechanism on radical-radical cross-coupling reaction through photo-redox of semiconductor-type porous materials, but also opens up a door

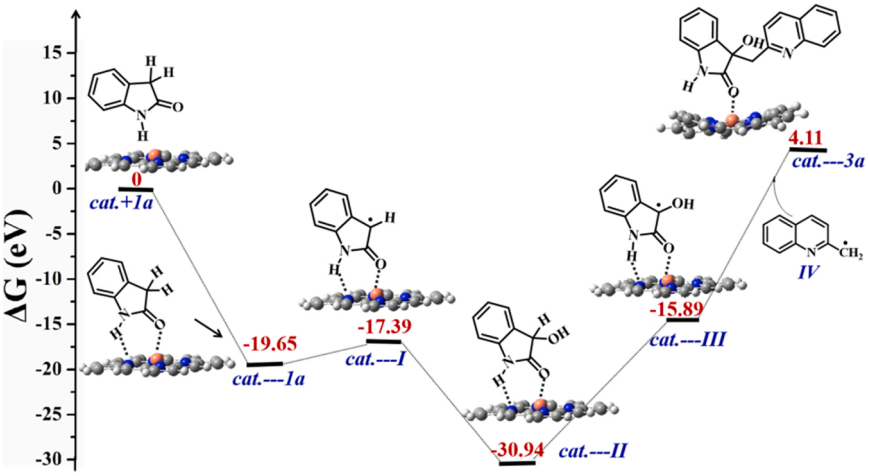

Scheme 3. The profile of Gibbs free energies at 298.15 K for oxidative-coupling reaction.

Table 2
Reaction scope of indolin-2-ones and 2-methyl-substituted N-heteroarenes.[a,b].

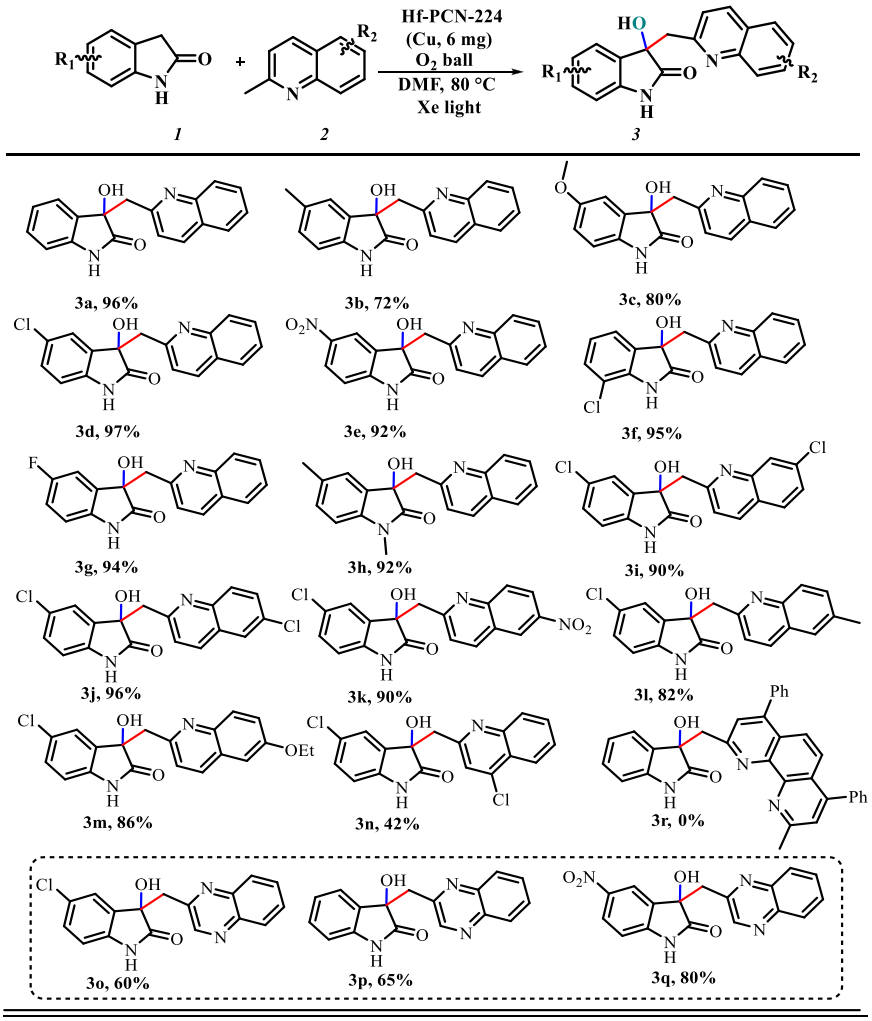

Reaction condition: **1** (0.2 mmol), **2** (0.24 mmol, 1.2 eq), Hf-PCN-224(Cu, 1200 nm, 6 mg), DMF (1 mL), 80 °C, 300 W Xe lamp with a UV-cut off filter, $\lambda > 380$ nm, O_2 ball; *[b]* Isolated yields;

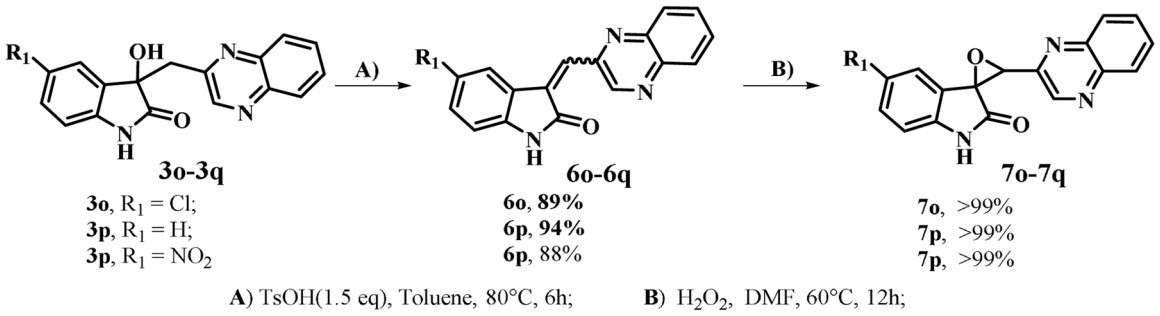

Scheme 4. The synthesis of anti-neuroblastoma agents.

for difunctionalization of C(sp^3)-H bond in laboratories and factories.

CRediT authorship contribution statement

Zhiyong Tang proposed the research direction and guided the project. Lingjuan Zhang conceived and performed most of the experiments. Lijuan Ma carried out DFT calculation and Jincong Yuan helped in characterizations of catalysts. Lingjuan Zhang, Xian-Ming Zhang and Zhiyong Tang analyzed the experimental results and drafted the manuscript.

Declaration of Competing Interest

The authors declare that they have no known competing financial interests or personal relationships that could have appeared to influence the work reported in this paper.

Data Availability

Data will be made available on request. All data needed to evaluate the conclusions in the paper are present in the paper and/or the Supplementary Materials.

Acknowledgements

This work was supported by NSFC (No. 22275118), the 1331 Engineering of Shanxi Province, Basic research project of Shanxi Province (201901D211392).

Appendix A. Supporting information

Supplementary data associated with this article can be found in the online version at doi:10.1016/j.apcatb.2022.122049.

References

[1] a) C.-Y. Huang, J.B. Li, C.-J. Li, Chem. Sci. 13 (2022) 5465–5504;
b) H. Yi, G.T. Zhang, H.M. Wang, Z.Y. Huang, J. Wang, A.K. Singh, A.W. Lei, Chem. Rev. 117 (2017) 9016–9085.
[2] a) L. Capaldo, D. Ravelli, M. Fagnoni, Chem. Rev. 122 (2022) 1875–1924;
b) H. Cao, X.X. Tang, H.D. Tang, Y. Yuan, J. Wu, Chem. Catal. 1 (2021) 523–598.
[3] a) Q.-Y. Meng, T.E. Schirmer, A.L. Berger, K. Donabauer, B. König, J. Am. Chem. Soc. 141 (2019) 11393–11397;
b) R. Zhou, H.W. Liu, H.R. Tao, X.J. Yu, J. Wu, Chem. Sci. 8 (2017) 4654–4659.
[4] a) Y. Zhao, J.-H. Lin, X.-C. Hang, J.-C. Xiao, J. Org. Chem. 83 (2018) 14120–14125;
b) L.L. Zhou, H. Yi, L. Zhu, X.T. Qi, H.P. Jiang, C. Liu, Y.Q. Feng, Y. Lan, A.W. Lei, Sci. Rep. 5 (2015), 15934-15934.
[5] a) J.W. Greenwood, B.T. Boyle, A. Mcnally, Chem. Sci. 12 (2021) 10538–10543;
b) Y.L. Shen, N. Lei, C. Lu, D.L. Xi, X.X. Geng, P. Tao, Z.S. Su, K. Zheng, Chem. Sci. 12 (2021) 15399–15406.
[6] a) C. Liu, N. Shen, R. Shang, Nat. Commun. 13 (2022) 354–361;
b) F. Juliá, T. Constantin, D. Leonori, Chem. Rev. 122 (2022) 2292–2352;
c) S.F. Zhou, K. Lv, R. Fu, C.L. Zhu, X.G. Bao, A.C.S. Catal 11 (2021) 5026–5034;
d) Y.G. Chen, X. Wang, X. He, Q. An, Z.W. Zuo, J. Am. Chem. Soc. 143 (2021) 4896–4902;
e) D.H. Wang, C. Mück-Lichtenfeld, A. Studer, J. Am. Chem. Soc. 142 (2020) 9119–9123;
f) M.-C. Fu, R. Shang, B. Zhao, B. Wang, Y. Fu, Science 63 (2019) 1429–1434.
[7] a) K. Minami, K. Ohmatsu, T. Ooi, A.C.S. Catal 12 (2022) 1971–1976;
b) I.N.-M. Leibler, M.A. Tekle-Smith, A.G. Doyle, Nat. Commun. 12 (2021) 6950–6959;
c) T. Shen, T.H. Lambert, Science 371 (2021) 620–626;
d) Q.M. Yang, Y.-H. Wang, Y.S. Qiao, M. Gau, P.J. Carroll, P.J. Walsh, E. J. Schelter, Science 372 (2021) 847–852;
e) L. Troian-Gautier, M.D. Turlington, S.A.M. Wehlin, A.B. Maurer, M.D. Brady, W. B. Swords, G.J. Meyer, Chem. Rev. 119 (2019) 4628–4683.
[8] a) H. Huang, Z.M. Strater, T.H. Lambert, J. Am. Chem. Soc. 142 (2020) 1698–1703;
b) J.B. McManus, J.D. Griffin, A.R. White, D.A. Nicewicz, J. Am. Chem. Soc. 142 (2020) 10325–10330;
c) T. Ide, J.P. Barham, M. Fujita, Y. Kawato, H. Egami, Y. Hamashima, Chem. Sci. 9 (2018) 8453–8460.
[9] a) K.F. Zhang, H.X. Chen, Y.X. Liu, J.G. Deng, L. Jing, A. Rastegarpanah, W.B. Pei, Z. Han, H.X. Dai, Appl. Catal. B: Environ. 315 (2022) 121545–121553;
b) H.C. Hao, L. Zhang, W.Z. Wang, S.W. Zeng, Catal. Sci. Technol. 8 (2018) 1229–1250;
c) H. Kisch, Acc. Chem. Res 50 (2017) 1002–1010.
[10] a) J. Qiao, Z.-Q. Song, C. Huang, R.-N. Ci, Z. Liu, B. Chen, C.-H. Tung, L.-Z. Wu, Angew. Chem. Int. Ed. 60 (2021) 27201–27205;
b) C. Huang, R.-N. Ci, J. Qiao, X.-Z. Wang, K. Feng, B. Chen, C.-H. Tung, L.-Z. Wu, Angew, Chem. Int. Ed. 60 (2021) 11779–11783;
c) C. Huang, J. Qiao, R.-N. Ci, X.-Z. Wang, Y. Wang, J.-H. Wang, B. Chen, C.-H. Tung, L.-Z. Wu, Chem 7 (2021) 1244–1257.
[11] Y. Nosaka, A.Y. Nosaka, Chem. Rev. 117 (2017) 11302–11336.
[12] a) J. Guo, Y.T. Qin, Y.F. Zhu, X.F. Zhang, C. Long, M.T. Zhao, Z.Y. Tang, Chem. Soc. Rev. 50 (2021) 5366–5396;
b) A. Bavykina, N. Kolobov, I.S. Khan, J.A. Bau, A. Ramirez, J. Gascon, Chem. Rev. 120 (2020) 8468–8535;
c) Y.-S. Wei, M. Zhang, R.Q. Zou, Q. Xu, Chem. Rev. 120 (2020) 12089–12174;
d) Q. Wang, D. Astruc, Chem. Rev. 120 (2019) 1438–1511;
e) L. Jiao, Y. Wang, H.L. Jiang, Q. Xu, Adv. Mater. 30 (2018) 1703663–1703685.
[13] T. Luo, L.L. Li, Y.L. Chen, J. An, C.C. Liu, Z. Yan, J.H. Carter, X. Han, A. M. Sheveleva, F. Tuna, E.J.L. McInnes, C.C. Tang, M. Schroder, S.H. Yang, Nat. Commun. 12 (2021) 3583–3592.
[14] Y. Zhang, J. Guo, J.W. Zhang, X.Y. Qiu, X.F. Zhang, J.Y. Han, B.H. Zhang, C. Long, Y.N. Shi, Z.J. Yang, W.S. Zhao, Z.Y. Tang, Chem 8 (2022) 1688–1704.
[15] a) L. Kimberley, A.M. Sheveleva, J.N. Li, J.H. Carter, X.C. Kang, G.L. Smith, X. Han, S.J. Day, C.C. Tang, F. Tuna, E.J.L. McInnes, S.H. Yang, M. Schroder, Angew. Chem. Int. Ed. 60 (2021) 15243–15247;
b) X. Gong, Y.F. Shu, Z. Jiang, L.X. Lu, X.H. Xu, C. Wang, H.X. Deng, Angew. Chem. Int. Ed. 59 (2020) 5326–5331;
c) J.-D. Xiao, H.L. Jiang, Acc. Chem. Res. 52 (2019) 356–366;
d) Y.-X. Tan, S.-X. Lin, C.P. Liu, Y.Y. Huang, M. Zhou, Q. Kang, D.Q. Yuan, M. C. Hong, Appl. Catal. B: Environ. 227 (2018) 425–432;
e) L. Zeng, X.Y. Guo, C. He, C.Y. Duan, ACS Catal. 6 (2016) 7935–7947.
[16] Sonam Varun, R. Kakkar, Med Chem, Comm 10 (2019) 351–368.
[17] a) R.-M. Hu, D.-Y. Han, N. Li, J. Huang, Y. Feng, D.-Z. Xu, Angew. Chem. Int. Ed. 59 (2020) 3876–3880;
b) Y.-H. Lai, R.-S. Wu, J. Huang, J.-Y. Huang, D.-Z. Xu, Org. Lett. 22 (2020) 3825–3829.
[18] T.H. Chang, C.W. Kung, H.W. Chen, T.Y. Huang, S.Y. Kao, H.C. Lu, M.H. Lee, K. M. Boopathi, C.W. Chu, K.C. Ho, Adv. Mater. 27 (2015) 7229–7235.
[19] A.D. Becke, J. Chem. Phys. 107 (1997) 8554–8560.
[20] A.D. Becke, J. Chem. Phys. 98 (1993) 5648–5652.
[21] M.P. Andersson, P. Uvdal, J. Phys. Chem. A 109 (2005) 2937–2941.
[22] a) L. Shi, L.Q. Yang, H.B. Zhang, K. Chang, G.X. Zhao, T. Kako, J.H. Ye, Appl. Catal. B: Environ. 224 (2018) 60–68;
b) Y.X. Wang, H. Cui, Z.-W. Wei, H.-P. Wang, L. Zhang, C.-Y. Su, Chem. Sci. 8 (2017) 775–780;
c) D.W. Feng, W.-C. Chung, Z.W. Wei, Z.-Y. Gu, H.-L. Jiang, Y.-P. Chen, D. J. Darensbourg, H.-C. Zhou, J. Am. Chem. Soc. 135 (2013) 17105–17110.d)the CCDC number: 2195842.
[23] J.W. Liu, Y.-Z. Fan, X. Li, Z.W. Wei, Y.-W. Xu, L. Zhang, C.-Y. Su, Appl. Catal. B: Environ. 231 (2018) 173–181.
[24] a) F.Y. Li, D. Tian, Y.F. Fan, R. Lee, G. Lu, Y.L. Yin, B.K. Qiao, X.W. Zhao, Z. W. Xiao, Z.Y. Jiang, Nat. Commun. 10 (2019) 1774–1782;
b) S. Paria, H.-J. Lee, K. Maruoka, A.C.S. Catal 9 (2019) 2395–2399;
c) T.D. Shi, S.H. Teng, Y.J. Wei, X. Guo, W.H. Hu, Green. Chem. 21 (2019) 4936–4940;
d) J. Wang, Z.-X. Deng, C.-M. Wang, P.-J. Xia, J.-A. Xiao, H.-Y. Xiang, X.-Q. Chen, H. Yang, Org. Lett. 20 (2018) 7535–7538;
e) K. Mishra, T.N. Poudel, N. Basavegowda, Y.R. Lee, J. Catal 344 (2016) 273–285.
[25] a) Z.D. Tan, S.B. Zhu, Y.B. Liu, X.M. Feng, Angew. Chem. Int. Ed. 61 (2022), e202203374;
b) K.J. Liang, N. Li, Y. Zhang, T. Li, C.F. Xia, Chem. Sci. 10 (2019) 3049–3053;
c) Q.G. Chen, L.H. Xie, Z.J. Li, Y. Tang, P. Zhao, L.L. Lin, X.M. Feng, X.H. Liu, Chem. Commun. 54 (2018) 678–681;
d) M. Montesinos-Magraner, C. Vila, R. Cantón, G. Blay, I. Fernández, M. C. Muñoz, J.R. Pedro, Angew. Chem. Int. Ed. 54 (2015) 6320–6324.
[26] L.J. Zhang, J.C. Yuan, L.J. Ma, Z.Y. Tang, X.-M. Zhang, J. Catal 401 (2021) 63–69.
[27] M. Montana, F. Correard, O. Khoumeri, M.A. Esteve, T. Terme, P. Vanelle, Molecules 19 (2014) 14987–14998.